The Astrophysical Journal, 802:18 (16pp), 2015 March 20 doi:10.1088/0004-637X/802/1/18
© 2015. The American Astronomical Society. All rights reserved.

WEIGHING GALAXY DISKS WITH THE BARYONIC TULLY–FISHER RELATION

Stacy S. McGaugh[1] and James M. Schombert[2]
[1] Department of Astronomy, Case Western Reserve University, Cleveland, OH 44106, USA; stacy.mcgaugh@case.edu
[2] Department of Physics, University of Oregon, Eugene, OR 97403, USA; jschombe@uoregon.edu
Received 2014 February 27; accepted 2015 January 26; published 2015 March 16

ABSTRACT

We estimate the stellar masses of disk galaxies with two independent methods: a photometrically self-consistent color–mass-to-light ratio relation (CMLR) from population synthesis models, and the baryonic Tully–Fisher relation (BTFR) calibrated by gas-rich galaxies. These two methods give consistent results. The CMLR correctly converts distinct Tully–Fisher relations in different bands into the same BTFR. The BTFR is consistent with $M_b \propto V_f^4$ over nearly six decades in mass, with no hint of a change in slope over that range. The intrinsic scatter in the BTFR is negligible, implying that the IMF of disk galaxies is effectively universal. The gas-rich BTFR suggests an absolute calibration of the stellar mass scale that yields nearly constant mass-to-light ratios in the near-infrared (NIR): 0.57 $M_\odot/L_\odot$ in K_s and 0.45 $M_\odot/L_\odot$ at 3.6 μm. There is only modest intrinsic scatter (∼0.12 dex) about these typical values. There is no discernible variation with color or other properties: the NIR luminosity is a good tracer of stellar mass.

Key words: galaxies: evolution – galaxies: fundamental parameters – galaxies: kinematics and dynamics – galaxies: photometry – galaxies: stellar content

1. INTRODUCTION

The stellar mass of a galaxy is one of its most fundamental characteristics. Based on our knowledge of stellar evolution, we expect to be able to use measured galaxy luminosity and color to estimate stellar mass (e.g., Bell & de Jong 2001; Bell et al. 2003; Portinari et al. 2004; Zibetti et al. 2009; Into & Portinari 2013). However, population synthesis models remain uncertain (Conroy & Gunn 2010), and are not always self-consistent (McGaugh & Schombert 2014).

Despite considerable progress, a variety of difficult issues persist. The star formation history of unresolved populations is difficult to constrain uniquely. The contribution to the integrated luminosity of bright but short-lived stars in late stages of evolution remains uncertain (e.g., asymptotic giant branch (AGB) stars: Maraston 2005; Marigo et al. 2008; Kriek et al. 2010; Melbourne et al. 2012; Zibetti et al. 2013). The distribution of stellar metallicity as well as the mean value appears to play an important role (Schombert & Rakos 2009; Conroy & Gunn 2010; Schombert & McGaugh 2014a, 2014b). Stellar mass estimates can depend considerably on the treatment of these effects.

The largest persistent uncertainty is in the mass spectrum of stars (the initial mass function (IMF)). Most of the light is produced by massive stars while most of the integrated mass resides in low-mass stars. Consequently, small differences in the IMF can have large effects on the stellar mass-to-light ratio, Υ_*. Such variations would lead to substantial scatter in the Tully–Fisher relation (Tully & Fisher 1977), which is not observed. This implies that the galaxy-averaged IMF does not vary wildly (McGaugh et al. 2000; Verheijen 2001).

Methods to estimate stellar mass that are independent of the IMF would be helpful. One approach to this problem is to measure the vertical velocity dispersion in face-on disk galaxies (e.g., Bershady et al. 2010, 2011). Another is provided by the baryonic Tully–Fisher relation (BTFR). This is one of the strongest correlations in extragalactic astronomy (McGaugh 2005), providing an empirical link between mass and observed rotation velocity.

Recent work on gas-dominated galaxies (Begum et al. 2008; Swaters et al. 2009; Stark et al. 2009; Trachternach et al. 2009) has made it possible to obtain an absolute calibration of the mass scale of the BTFR that is largely independent of stellar mass estimates (McGaugh 2012). When the gas mass exceeds the stellar mass, the systematic error in the stellar mass induced by the IMF, etc., becomes a minor contributor to the error budget (McGaugh 2011). The assumptions necessary in population models cease to be the dominant factor in the calibration of the BTFR.

Here we examine a sample of galaxies with high-quality, extended rotation curves from 21 cm interferometry and photometry in the optical and near-infrared (NIR) (Section 2). We first construct the luminous Tully–Fisher relation (LTFR) for each band, and the corresponding stellar mass Tully–Fisher (STFR) relation and BTFR using self-consistent stellar population mass-to-light estimators (Section 3). We then estimate the stellar mass of each galaxy using the BTFR independently calibrated by gas-rich galaxies (Section 4), and use this as a check on the IMF (Section 5). We compare these results and discuss their consistency (or lack thereof) with other methods (Section 6), and summarize in Section 7.

2. DATA

The data used here are based on the sample of galaxies with extensive photometry in optical and NIR bands assembled by McGaugh & Schombert (2014). All galaxies employed here have been observed at B, V, and [3.6]. Many, though not all, also have I, J, and K_s-band data. Many SINGS (Kennicutt et al. 2003; Dale et al. 2005) galaxies observed as part of the THINGS (Walter et al. 2008) HI survey are utilized. The sample further includes many new *Spitzer* observations (Schombert & McGaugh 2014b). These data are used to estimate the luminosity and stellar mass of each galaxy.

We select galaxies from McGaugh & Schombert (2014) for which credible measurements of the outer, flat rotation velocity V_f are available from 21 cm interferometry. This measure provides the best available estimate of the characteristic

rotation velocity of disk galaxies in the sense that it minimizes the scatter in the Tully–Fisher relation (Verheijen 2001; McGaugh 2005). The more commonly employed line-width is less precise, in that it results in a larger irreducible scatter in the BTFR (Verheijen 2001; McGaugh 2012; Zaritsky et al. 2014). This difference is critical for estimating stellar masses from the BTFR, as uncertainty in the rotation velocity propagates strongly into the implied mass.

We selected galaxies for observation with *Spitzer* (Schombert & McGaugh 2014b) to extend the dynamic range over which the BTFR could be constructed. Galaxies with existing high-quality HI rotation curves were selected to supplement the THINGS sample (Walter et al. 2008) at both ends of the BTFR. The resulting sample extends to both greater and lower luminosity than present in THINGS. The aim was to cover as much range in mass as possible with evenly sampled bins. This is done to avoid the common selection effects afflicting magnitude-limited samples, which typically have many L^* galaxies but few or none with $L < 10^9\ L_\odot$. The result is a sample of galaxies that probes the BTFR over a large dynamic range in a uniform way, free of the usual bias in which the region around L^* is probed many times, while either end of the relation is underrepresented.

The emphasis here is to uniformly sample as much of the BTFR as possible with the highest-quality data available. In this vein, we require that galaxies be sufficiently inclined that sin (i) corrections are modest ($i > 45°$; see the discussion in Stark et al. 2009). This excludes a number of THINGS galaxies with otherwise good data (e.g., NGC 6946). We also exclude two galaxies for which we do not entirely trust the data: NGC 2841 and NGC 2903. NGC 2841 is a well-known outlier from the Tully–Fisher relation (Bottema et al. 2002). Whether NGC 2841 is a true outlier, or some systematic error is to blame, is beyond the scope of this paper. However, it is not simply at one extreme of the scatter; it sits well away from all other data. We therefore suspect some systematic error is to blame. In the case of NGC 2903, the [3.6] photometry is suspect. De Blok et al. (2008) note problems constructing a mass model, and the resulting [3.6] magnitude makes NGC 2903 an outlier from both the (V – [3.6], [3.6]) color–magnitude relation (Schombert & McGaugh 2014a) and the [3.6] Tully–Fisher relation, even though it does not deviate from the Tully–Fisher relation in other bands, including K_s. We therefore infer that the [3.6] magnitude of NGC 2903 is not reliable, so we do not consider it further.

The final sample contains 26 galaxies spanning the range $50 \lesssim V_f \lesssim 300$ km s^{-1}, $3 \times 10^7 \lesssim M_* \lesssim 3 \times 10^{11}\ M_\odot$, and $10^8 \lesssim M_g \lesssim 5 \times 10^{10}\ M_\odot$. It spans four decades in luminosity, while magnitude-limited Tully–Fisher samples typically span two (e.g., Pizagno et al. 2007). This large dynamic range is more important for constraining the slope of the BTFR than is the sheer numbers of galaxies.

Sample selection is driven by data quality: it is constructed to be as free of systematic errors as possible. Of course, one can never completely exclude the presence of systematic errors. The two that concern us most are residual systematic errors in the adopted distances and in the inclination determinations.

Direct distance measurements via Cepheids or the tip of the red giant branch are adopted when available (Tully et al. 2009). When no direct measurement is available, we adopt a Hubble flow estimate consistent with independent local galaxy data ($H_0 = 75$ km s^{-1} Mpc^{-1}: Sorce et al. 2012). Galaxies lacking direct measurements tend to be the most distant, luminous galaxies or the less studied dwarfs—i.e., those at the extremes of the relation. Dividing the sample into those objects with and without direct distance determinations reveals no statistically significant difference: we recover the local distance scale. If instead $H_0 = 67$ km s^{-1} Mpc^{-1}, the primary systematic effect would be to increase our mass estimates by 0.1 dex with a corresponding translation of the BTFR zero point.

The effects of systematic inclination errors are discussed at length by McGaugh (2012). These most commonly manifest as outliers to the low-velocity side of the BTFR. Oval distortions can make galaxies look less face-on than they are, so the inclination correction may be underestimated. This is mitigated here by the use of velocity fields, which give an additional constraint on the inclination. As we will see, the scatter around the BTFR relation is small with no obvious asymmetry, so systematic inclination errors appear to be small in this sample.

Fundamental data like distances, magnitudes, and colors are given in McGaugh & Schombert (2014). Data specific to our present analysis are given in Table 1. Column 1 gives the name of the galaxy. Column 2 gives the rotation velocity V_f. Columns 3 and 4 give the atomic and molecular gas masses, respecively. Luminosities in each of the V, I, and [3.6] bands are given in columns 5–7. As in McGaugh & Schombert (2014), we adopt solar absolute magnitudes of 4.83, 4.08, and 3.24 in the V, I, and [3.6] bands. References to the sources of the data are given in column 8.

Rotation curves generally experience an extended radial range over which the rotation velocity is approximately constant. This flat velocity, V_f, is an obvious measure of the characteristic global rotation speed of a galaxy. We have measured or remeasured anew V_f for all galaxies considered here by taking the mean of data along the outer, flat portion of the rotation curve. While the outer parts of rotation curves are very nearly flat, they are not perfectly so. We implemented several algorithms for deciding what constitutes the flat portion of the rotation curve: a subjective estimate by eye, a definition by slope such that $\partial \log V/\partial \log R < 0.1$ (McGaugh 2005; Stark et al. 2009; Swaters et al. 2009), and an outlier rejection routine that iteratively excludes points from the rising or falling portion of the rotation curve. These methods yield consistent results within the errors. Indeed, the relative variation around V_f along a rotation curve, while clearly perceptible, is typically smaller than the absolute uncertainty in V_f: $\Delta V = \Delta R(\partial V/\partial R) < \sigma_V$. Hence the mildly non-zero slopes $\partial V/\partial R$ that are observed do not preclude accurate measurement of V_f. A greater concern is the occasional warp that causes a radial variation in the inclination within a galaxy. Indeed, this might be one issue in NGC 2841. The galaxy for which this concern is most important in the present sample is DDO 154 (see the discussion in de Blok et al. 2008).

The gas mass of each galaxy is adopted from the corresponding tabulated reference in Table 1. The HI mass is obtained from the 21 cm flux in the usual fashion: $M(\mathrm{HI}) = 2.36 \times 10^5 D^2 F_{\mathrm{HI}}$. The molecular gas mass has been estimated for the THINGS galaxies by Leroy et al. (2008), who discuss in detail the conversion from observed CO flux to H_2 mass.

Many galaxies lack CO detections. In these cases, we exploit the near-constant efficiency of star formation observed by Leroy et al. (2008) to estimate the molecular

Table 1
Rotation Velocities and Gas Masses

Galaxy	V_f (km s^{-1})	M (HI) ($10^9\ M_\odot$)	$M(H_2)$ ($10^9\ M_\odot$)	L_V ($10^9\ L_\odot$)	L_I ($10^9\ L_\odot$)	$L_{[3.6]}$ ($10^9\ L_\odot$)	References
DDO 154	53.3 ± 4.7	0.0925	0.00618	0.0516	0.0294	0.0725	1,2,3,4,5
D631-7	52.9 ± 5.0	0.147	0.0127	0.0540	0.0448	0.0975	1,2,3,6
DDO 168	53.4 ± 2.5	0.317	0.00279	0.166	...	0.187	1,2,3,7
D500-2	68.1 ± 6.6	0.871	0.00790	0.304	0.226	0.395	1,2,6
NGC 2366	59.7 ± 10.3	0.600	0.123	0.456	0.369	0.716	1,5,8
IC 2574	76.7 ± 4.5	1.41	0.0937	1.04	0.956	2.33	1,5,8
F563-1	111. ± 10.	3.50	0.0900	1.13	1.25	2.84	1,2,3,7
NGC 2976	86.0 ± 3.5	0.134	0.121	1.13	1.05	3.19	1,4,5
F568-V1	124. ± 10.	3.93	0.134	2.36	2.25	4.20	1,2,3,7
NGC 1003	113.5 ± 1.9	5.31	0.243	2.76	...	5.91	1,4,5
F568-1	116. ± 10.	4.02	0.141	3.10	2.98	7.10	1,2,3,9
NGC 7793	110.4 ± 4.4	0.761	0.282	2.99	1.80	7.55	1,4,5
UGC 128	131. ± 10.	6.51	0.420	4.49	4.20	11.3	1,2,3,10,11
NGC 2403	135.8 ± 4.0	2.52	0.522	3.86	5.00	12.1	1,4,5,10,11
NGC 925	113.6 ± 6.3	3.99	0.826	8.35	8.35	15.8	1,4,5
NGC 3198	148.9 ± 4.2	0.134	1.30	12.4	15.8	31.2	1,4,5
NGC 3621	152.3 ± 3.2	6.98	7.06	6.74	7.11	33.1	1,4,5
NGC 3521	191.9 ± 17.6	4.48	1.65	15.6	23.2	91.1	1,4,5
NGC 3031	199.0 ± 13.8	6.97	1.58	23.0	38.7	106.	1,4,5
NGC 5055	181.1 ± 11.9	7.21	2.36	26.3	40.2	135.	1,4,5
NGC 2998	211.7 ± 2.7	27.7	7.27	74.8	...	160.	1,7
NGC 6674	240.5 ± 4.2	38.2	9.30	63.2	...	230.	1,7
NGC 7331	245.8 ± 8.4	9.38	4.30	38.3	67.1	259.	1,4,5
NGC 801	218.8 ± 3.5	36.7	12.0	71.5	...	268.	1,7
NGC 5533	239.9 ± 5.0	23.5	13.9	62.7	...	303.	1,7
UGC 2885	298. ± 10.	34.5	15.7	179.	...	468.	1,7

Note. Galaxies are listed in order of increasing [3.6] luminosity as in McGaugh & Schombert (2014).
References (1) McGaugh & Schombert (2014), (2) Schombert & McGaugh (2014b), (3) Schombert et al. (2011), (4) de Blok et al. (2008), (5) Leroy et al. (2008), (6) Trachternach et al. (2009), (7) McGaugh (2005), (8) Oh et al. (2008), (9) de Blok et al. (1996), (10) de Blok & McGaugh (1996), (11) Verheijen & de Blok (1999).

gas mass from the observed star formation rate (Schombert et al. 2011). This method implicitly corrects for the metallicity dependence of the CO–H_2 conversion factor, albeit by assuming a constant star formation efficiency. For galaxies lacking CO detections, we estimate the molecular gas mass as

$$\log\left[M\left(\mathrm{H_2}\right)\right] = \log\left(\mathrm{SFR}\right) + 9.15. \quad (1)$$

Here, the molecular gas mass is in solar masses and the star formation rate (SFR) is in $M_\odot$ yr^{-1}. These estimates are rather uncertain (compare to other estimators discussed by McGaugh 2012), but the molecular gas mass is usually a small portion of the mass budget, and makes little difference to the result.

The luminosities given in Table 1 are computed directly from the distances, magnitudes, and colors given in McGaugh & Schombert (2014). The [3.6] luminosities originate either with de Blok et al. (2008) or Schombert & McGaugh (2014b), with other bands as cited in the table. The formal uncertainties in the measured magnitudes are small, of the order of 0.02 mag. The dominant uncertainty in the luminosity and the gas mass is the distance. We treat the uncertainties in the luminosities as negligibly small, and consider the random distance uncertainties as a contributor to the scatter in the Tully–Fisher relations we construct.

3. DIRECT FITS

3.1. Types of Tully–Fisher Relations

The term "Tully–Fisher relation" has been used to mean a variety of subtly different things. Most commonly, the Tully–Fisher relation is posed as a relation between absolute magnitude and line-width (Tully & Fisher 1977) and employed as a distance indicator (e.g., Sorce et al. 2012). Here we construct several distinct flavors of Tully–Fisher relations from the assembled data in hopes of identifying the underlying physical basis of the relation.

We start with the relation between luminosity and asymptotic rotation velocity in each band. This is analogous to the common Tully–Fisher relation, but differs from it in that V_f from extended, resolved rotation curves is used rather than line-widths. While similar, these are not identical measures of the characteristic rotation velocity of a galaxy. The primary consequence is a systematic difference in the slopes of the fitted relation. Line-widths are sensitive to the presence of inner humps in rotation curves, which are prominent in luminous galaxies but largely absent in faint ones (see, e.g., Verheijen 2001; Noordermeer & Verheijen 2007). This causes the L–W relation to be shallower than the L–V_f relation, which we will refer to as the LTFR.

Next, we construct the STFR. We employ stellar population models to estimate the stellar mass of each galaxy based on their observed luminosities and the color–mas-to-light ratio

relation (CMLR) of McGaugh & Schombert (2014). We then construct the STFR implied independently by the luminosity observed in each band pass. If the our semi-empirical CMLR are correct, then each band's LTFR should transform into the same STFR.

Finally, we construct the BTFR. This is a relation between rotation velocity and baryonic mass (McGaugh et al. 2000; Bell & de Jong 2001; Verheijen 2001; McGaugh 2005; Pfenniger & Revaz 2005), where now the mass includes all observed forms of baryonic mass, stars, and gas: $M_b = M_* + M_g$. Again, if all is well, the same relation should be obtained independently from each band. We can also compare the result to that obtained independently from fitting gas-rich galaxies, which is very nearly independent of the stellar mass estimate (McGaugh 2011, 2012). The LTFR, STFR, and BTFR are shown in Figure 1.

The use of V_f as the velocity measure rather than line-widths leads to systematically steeper slopes for all flavors of the relation. For the BTFR, McGaugh (2012) found a slope $x = 3.41 \pm 0.08$ when line-widths are employed as the velocity measure, consistent with the 3.5 ± 0.2 reported independently by Zaritsky et al. (2014). In contrast, the slope of the BTFR is very close to 4 when V_f is employed as the measure of rotation velocity (Stark et al. 2009). It also consistently yields relations with lower scatter. For example, McGaugh (2012) estimates an irreducible scatter of ~0.2 dex in mass in the BTFR when line-widths are employed, but negligible intrinsic scatter with V_f.

3.2. Fitting

For the various possible ordinates of the Tully–Fisher relation, we fit relations of the form

$$\log\left(\ell\right) = \log A + x \log\left(V_f\right). \quad (2)$$

Here A is the normalization of the relation ($\log A$ being the intercept in the log–log plane) and x is the slope. The symbol ℓ represents any of the luminosity, stellar mass, gas mass, or baryonic mass, while V_f is of course the rotation velocity measured in the outer portion of the resolved rotation curve.

To fit the data here, we use the maximum likelihood method of Weiner et al. (2006). This allows for a finite intrinsic scatter in the ordinate in addition to random errors in both dimensions. The uncertainty that we estimate in the abscissa V_f is given in Table 1. The error in luminosity is dominated by uncertainty in distance rather than in apparent magnitudes. The uncertainty in the distance to each galaxy is heterogenous and hard to quantify with confidence. We therefore treat it as a contributor to the scatter. The best-fit scatter found in this way is a combination of random errors and intrinsic scatter, placing an upper limit on the latter. The results of the fits are reported in Table 2.

The slope of the LTFR becomes progressively steeper as we go to progressively redder bands (Table 2), consistent with previous findings (Tully et al. 1998; Verheijen 2001). As one might expect, the [3.6] LTFR has less scatter and better determined fit coefficients than that in V or I. Nevertheless, we caution against overinterpreting the specifics of these LTFR fits given the high gas content of the slower rotators.

The LTFR found here are steeper than many published relations. This is expected, as the particular value of the fitted LTFR slope depends on the dynamic range of the data. As one goes to lower velocities, one finds more gas-rich galaxies. The luminosity progressively underestimates the mass, so these galaxies fall too low, steepening the fitted slope. The scatter in luminosity at a given velocity also goes up (Matthews et al. 1998). The precise value of the fitted slope therefore depends on both the dynamic range of the sample, and the happenstance of the gas fractions of the galaxies therein. Magnitude limited samples will be biased to lower slopes, as they will preferentially include brighter, lower gas fraction galaxies at a given V_f. This can be a strong effect, since it occurs at one end of the relation where relatively few points can have considerable leverage on the best-fit slope. In our sample, exclusion of the three slowest rotators (with $V_f \approx 50$ km s^{-1}) flattens the fitted slope perceptibly (if not significantly).

An important consequence of sample dependence is that there probably is no such thing as a universally correct LTFR. The "right" answer is unique to each sample. This effect is difficult to discern in most samples, which tend to lack galaxies with $V_f \lesssim 90$ km s^{-1} where the effect becomes pronounced. This may be enough to explain subtle differences in published calibrations. It may also introduce systematic errors in distance determinations, as one is sampling different parts of the relation at different distances. Fortunately, this effect will be small as long as only bright galaxies are utilized in both calibration and distance determination.

3.3. Stellar Mass

Stellar mass is a more fundamental physical quantity than luminosity. The LTFR can and does vary from band to band. These all presumably originate from the same STFR, with differences in the LTFR reflecting systematic variations in the stellar populations composing fast and slow rotators. From the color–magnitude relation, one would expect progressively steeper LTFR as one goes from blue to red bands, but these should all originate from one STFR.

The stellar mass is estimated from $M_* = \Upsilon_* L$ for each band with the mass-to-light ratio Υ_* estimated by population synthesis models. Many models currently in wide use do not pass a straightforward self-consistency test, in that stellar masses estimated from the luminosity in different pass bands for the same galaxy return wildly different results (McGaugh & Schombert 2014). By comparing data over a broad range, McGaugh & Schombert (2014) constructed empirically self-consistent color–Υ_* relations.

We employ the CMLR of McGaugh & Schombert (2014) to estimate Υ_* with $B - V$ colors, which we found to be the most sensitive to variations in stellar mass-to-light ratio among the available colors. To be specific, we adopt the model of Bell et al. (2003) modified to give self-consistent photometric results as quantified in Table 7 of McGaugh & Schombert (2014):

$$\log \Upsilon_*^V = -0.628 + 1.305(B - V)$$
$$\log \Upsilon_*^I = -0.275 + 0.612(B - V)$$
$$\Upsilon_*^{[3.6]} = 0.47 \quad (3)$$

As expected, the dependence of Υ_* on color becomes weaker as one goes to redder bands. It effectively disappears in the NIR, so we neglect the meaninglessly tiny color slope (–0.007) at [3.6].

We make this particular choice of model because the model of Bell et al. (2003) required the least modification of the various models considered. By construction, the V-band Υ_* indicator is identical to the original one of Bell et al. (2003), and is subject to the usual normalization uncertainty due to the

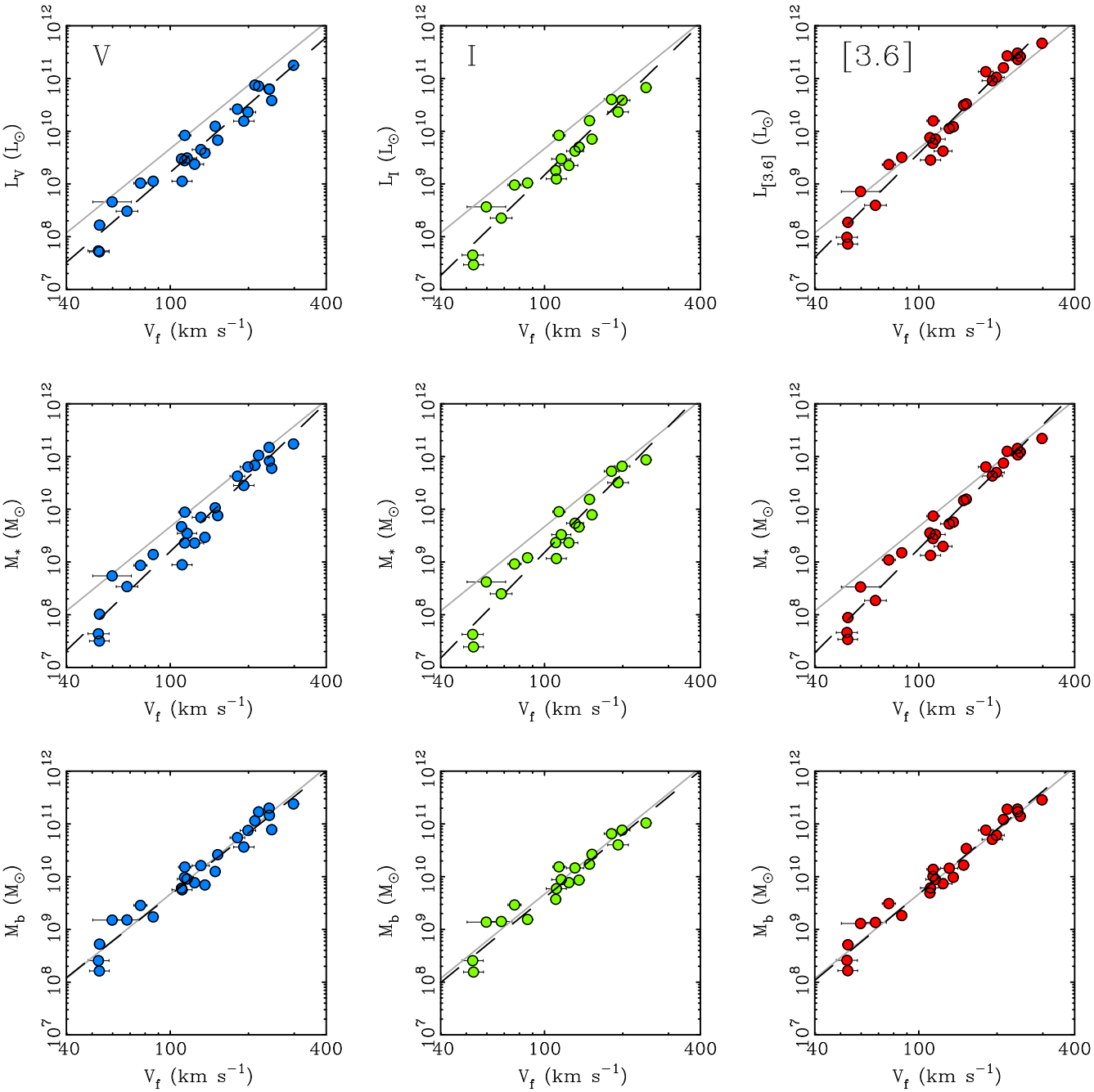

Figure 1. Tully–Fisher relations determined from *V* (left), *I* (middle), and [3.6] (right) data for the galaxies in Table 1. The top row shows the luminous Tully–Fisher relation (LTFR), the middle row the stellar mass Tully–Fisher relation (STFR), and the bottom row the baryonic Tully–Fisher relation (BTFR). In all cases the luminosity or mass is plotted against the flat, outer velocity. Fits to each relation are shown as dashed lines and reported in Table 2. For reference, the BTFR previously fit to gas-rich galaxies by McGaugh (2012) is shown as a light solid line in all panels.

IMF. Both the *I*-band and [3.6] Υ_* are modified to obtain photometric self-consistency. Requiring self-consistent stellar masses implies $0.4 < \Upsilon_*^{[3.6]} < 0.5$ for all models, including those that initially predicted rather different values. A constant NIR Υ_* is therefore a good approximation.

The dependence of the NIR Υ_* on color in Equation (3) is considerably weaker than the already weak relation anticipated in many models. This is required for self-consistency: the photometric data are not consistent with NIR mass-to-light ratios that depend much on color (see McGaugh & Schombert 2014). While there can certainly be some color dependence, the variation of $\Upsilon_*^{[3.6]}$ with color appears to be rather less than the intrinsic scatter in $\Upsilon_*^{[3.6]}$ from galaxy to galaxy, which itself is also fairly small.

In practice, the weak relation between NIR Υ_* and color means that NIR luminosity is a good proxy for stellar mass. One might hope to do better by fitting the entire spectral energy distribution (SED) of a galaxy, and this no doubt matters for extreme objects like those dominated by the light of very young stellar populations. However, for most galaxies, there is no value added from this procedure. Most of the information about Υ_* is contained in the first color ($B - V$ here), which is already negligible in the NIR. Further corrections from other colors carry progressively less information. In the case of [3.6] and the

Table 2
Tully–Fisher Relations and Their Scatter

Band	ℓ	x	$\log A$	$\sigma_{\log \ell}$
Luminous Tully–Fisher Relation				
V	L_V	4.27 ± 0.19	0.68 ± 0.41	0.18
I	L_I	4.77 ± 0.30	-0.37 ± 0.62	0.19
3.6	$L_{[3.6]}$	4.93 ± 0.17	-0.28 ± 0.36	0.15
Stellar Mass Tully–Fisher Relation				
V	M_*	4.70 ± 0.22	-0.20 ± 0.48	0.21
I	M_*	5.01 ± 0.31	-0.84 ± 0.64	0.20
3.6	M_*	4.93 ± 0.17	-0.61 ± 0.36	0.15
Baryonic Tully–Fisher Relation				
V	M_b	3.92 ± 0.18	1.81 ± 0.39	0.17
I	M_b	4.02 ± 0.24	1.56 ± 0.51	0.15
3.6	M_b	4.09 ± 0.15	1.49 ± 0.32	0.13
Gas-only Tully–Fisher Relation				
...	M_g	3.24 ± 0.28	2.89 ± 0.59	0.29

Note. Fits to the data in Table 1 of the form $\log \ell = \log A + x \log V_f$.

K_s-band, attempts at SED fitting are more likely to add noise than improve the estimate of Υ_*. Worse, they are prone to induce systematic errors from imperfections in the population models. For example, many models assume a single metallicity for the stellar population. This appears to be one driver for the predicted dependence of the NIR mass-to-light ratio on color being stronger than observed (McGaugh & Schombert 2014). Models with realistic metallicity distributions have a much weaker dependence of NIR Υ_* on color (Schombert & McGaugh 2014a).

If the stellar mass-to-light ratios estimated with Equation (3) are correct, the Υ_* for each band should succeed in converting the different LTFR observed for each independent band into the same STFR. This procedure is indeed successful. The STFR in Table 2 are equivalent within the errors.

Since the adopted NIR mass-to-light ratio is constant, the [3.6] STFR is identical to the [3.6] LTFR except for the change in normalization due to the non-unity value of the mass-to-light ratio. Consequently, it is the slope of the V and I LTFR that change to result in an STFR that matches that from [3.6]. This goes in the expected sense from the color–magnitude relation: fainter galaxies are bluer and have lower Υ_* on average. Use of incorrect CMLR would lead to discordant STFR in the various bands. That we find consistent SFTR provides independent confirmation that the CMLR in Equation (3) determined photometrically by McGaugh & Schombert (2014) are very nearly correct.

The conversion from the LTFR to the STFR can only work to the extent that $B - V$ is predictive of Υ_*. That it does work suggests that $B - V$ is an adequate Υ_* indicator. It certainly is not perfect: one expects a fair amount of scatter about the mean CMLR. The expected consequence is an increase in the scatter in the STFR relative to the LTFR. Even though the mean slope of the CMLR succeeds in converting the LTFR into the STFR, the scatter in the latter increases due to misestimates of the mass-to-light ratios of individual galaxies. That is, the scatter in the STFR should include whatever scatter is already in the LTFR, plus an extra component for the scatter in the CMLR. This effect does appear to be present in the data, as seen by the amount of scatter in Table 2.

From a population perspective, one expects a greater amount of scatter in Υ_* at bluer wavelengths. The scatter fit in Table 2 is a combination of intrinsic scatter and that from random errors like those in distance. While there is considerable uncertainty in these uncertainties, we estimate that random errors contribute ~0.08 dex to the scatter in the ordinate of the various Tully–Fisher relations. Subtracting this in quadrature from the fitted value for each band gives an estimate of the intrinsic scatter in Υ_*: 0.16 dex in V, 0.13 in I, and 0.12 in [0.36]. For comparison, Bell & de Jong (2001) anticipate 0.1 dex of scatter in K from variations in the star formation history alone, and Portinari et al. (2004) anticipate 0.15 dex.

It thus appears that the observed scatter is entirely explained by random errors plus the expected scatter in mass-to-light ratios. The scatter in Υ_* is consistent with that expected from the inevitable variations in star formation histories. This leaves essentially no room for variations in the IMF from galaxy to galaxy. Apparently, the IMF in disk galaxies is universal, at least averaged over the many star formation events that build a galactic disk over a Hubble time.

There is also precious little room for intrinsic scatter in whatever physics underlies the Tully–Fisher relation. Given the small size of the sample, we should not overinterpret the precise values of the scatter. However, it is not obvious that larger samples will inevitably lead to larger scatter, as they bring with them the larger risk of unaccounted systematic errors (see discussion in McGaugh 2012). Bear in mind that in order to increase the intrinsic scatter of this sample, we must have *overestimated* random errors. Even in the limit of zero experimental error and no scatter in Υ_*, the intrinsic scatter is still small (<0.15 dex; Table 2).

3.4. Gas Mass

The atomic and molecular gas masses given in Table 1 are used to compute the total gas mass

$$M_g = 1.33\left[M\left(\mathrm{HI}\right) + M\left(\mathrm{H_2}\right)\right]. \quad (4)$$

The factor 1.33 accounts for the mass in helium. One can debate the appropriate value of the second digit past the decimal, but not at a level that matters here. We adopt 1.33 for consistency with McGaugh (2012), whose BTFR calibration will be utilized in Section 4. The contribution of other gas phases is generally negligible, at least within the visible disk where all relevant quantities are measured.

Luminosity is the original ordinate of the Tully–Fisher relation. Stars are the dominant baryonic mass component of bright galaxies. We therefore do not expect there to be a meaningful gas-only Tully–Fisher relation. For completeness, we do construct one. It is shown in Figure 2.

At first glance, the relation in Figure 2 appears perfectly reasonable. It has considerably greater scatter than any of the STFR, but it is certainly possible to fit a line through the data (left panel of Figure 2). This is not particularly meaningful, as the scatter here is real. Galaxies of the same V_f can differ in gas mass by an order of magnitude.

Galaxies segregate by gas fraction (right panel of Figure 2). To estimate the gas fraction, we use $\Upsilon_*^{[3.6]} = 0.47$ from Equation (3) to estimate the stellar mass, and bin the data by

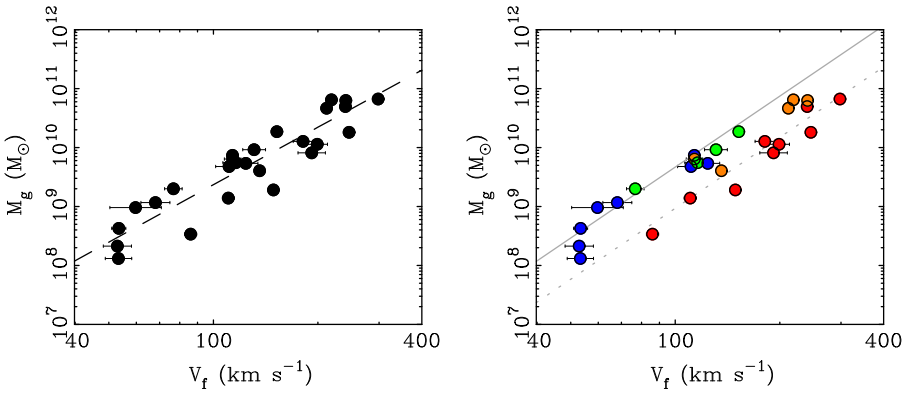

Figure 2. Gas-only Tully–Fisher relation. Gas mass is plotted against rotation velocity without any reference to stellar luminosity. The data are plotted and fit (dashed line) in the left panel (see Table 2 for coefficients). The fit looks reasonable, though the scatter is larger than in any of the LTFR. The right panel shows the same data, but with points color coded by gas fraction. To estimate the ratio M_*/M_g, we use $M_* = 0.47L_{[3.6]}$. Red points have $M_*/M_g > 2$, orange points $1 < M_*/M_g < 2$, green points $\frac{1}{2} < M_*/M_g < 1$, and blue points $M_*/M_g < \frac{1}{2}$. The data clearly segregate by gas fraction. Gas-rich galaxies follow the BTFR (solid gray line) while gas-poor galaxies fall well below it. For comparison, the dotted lines parallels the BTFR but is shifted by a factor of 5. This is the amplitude of the shift one would expect for a typical Milky Way-like spiral with a ∼20% gas fraction. The segregation by gas fraction renders meaningless the fit in the left panel.

the ratio M_*/M_g. Galaxies with $M_* < M_g$ hover near the BTFR previously fit to gas-rich galaxies (McGaugh 2012). Since stellar mass is ignored here, these should all fall slightly below the BTFR line. Most do, though a few fall a little too high, albeit within the errors. In contrast, galaxies with $M_* > M_g$ all fall well below the line. The obvious inference is that we are missing an important component of the mass in these galaxies: the stars. Indeed, the amount of the shift is what we expect for the typical gas fractions of bright spirals.

Just as we should not ignore the gas in faint galaxies, we should not ignore the stars in bright ones. Neither the LTFR nor the gas-only Tully–Fisher relation are fundamental. Instead, they must stem from a more basic relation that does not distinguish between mass in the form of stars or gas.

3.5. Baryonic Mass

In order to construct the BTFR, we take the sum of stellar and gas mass to obtain the baryonic mass

$$M_b = M_* + M_g. \quad (5)$$

The stellar mass is computed with Equation (3) and the gas mass is from Equation (4). The BTFR resulting from the stellar mass as computed from each of V, I, and [3.6] is shown in the bottom row of Figure 1.

If all has gone well, this BTFR should be consistent from band to band. This should necessarily follow if the STFR has been computed correctly for each band. Indeed, this is the case: the relations computed separately for each band are mutually consistent. Both the slopes and the intercepts are indistinguishable within the errors. This convergence is readily seen in Figure 1. These relations are also consistent with the BTFR previously fit to independent data for gas-rich, predominantly slow rotators by McGaugh (2012).

Another encouraging point is that scatter in the BTFR is less than that in either the LTFR or the STFR. Including the gas mass as well as the stellar mass has made a better relation in this sense. Indeed, the relation is near-perfect in the sense that their appears to be very little intrinsic scatter. In Section 3.3 we estimated the intrinsic scatter in stellar mass-to-light ratios for this sample to be 0.16 dex in V, 0.13 in I, and 0.12 in [0.36]. The scatter in the BTFR is 0.17 dex in V, 0.15 in I, and 0.13 in [0.36] (Table 2). These are effectively identical given the uncertainties, leaving precious little room for intrinsic scatter in the relation itself.

The fundamental, underlying physical relation appears to be one between baryonic mass and asymptotic rotation velocity. The data are consistent with a single power law (a single linear slope in log–log space) over four decades in baryonic mass. There is no evidence for a bend or break in the relation as sometimes anticipated by models (e.g., Trujillo-Gomez et al. 2011).

The luminosity of the traditional LTFR is merely a proxy for baryonic mass. This works well for bright spirals that are gas-poor, but starts to break down at lower velocity where galaxies tend to be more gas-rich. As a consequence, the LTFR suffers increased scatter at low rotation velocity, and may appear to bend. This simply illustrates the shortcomings of luminosity as a mass indicator, not any break in the underlying relation.

Since luminosity is an imperfect indicator of baryonic mass, calibrations of the LTFR are inevitably inaccurate at some level. Bright spirals do contain gas, and the gas fraction varies from galaxy to galaxy. The LTFR will inevitably deviate from the underlying BTFR in a way that depends both on the band pass and the gas fractions of the sample of calibration galaxies. Fortunately, this appears to be a minor effect for bright galaxies.

The small intrinsic scatter in the BTFR suggests that there is no large reservoir of missing baryons remaining to be discovered in the disks of spiral galaxies (McGaugh et al. 2000). It is obvious if we miss either the stars or the gas (Figures 1 and 2). If we were still missing a comparable number of baryons, then the sum in Equation (5) would be incomplete. This would show up as a systematic deviation from the BTFR, which is not apparent. One can always have *some* mass in an undetected component (e.g., in the form of very cold molecular gas—Pfenniger & Revaz 2005), but its mass must be $\ll M_b$ from Equation (5) so that the data stay within the scatter. Consequently, the stars and cold gas that we detect appear to compose the bulk of the baryonic mass in disk galaxies.

4. STELLAR MASSES FROM THE BTFR

Here we employ the BTFR as a method to estimate stellar mass. Rather than trust population synthesis models, we ask what the stellar mass must be in order for a galaxy to lie on the BTFR. This would obviously be a completely circular exercise if we were to use the BTFR calibrated with star-dominated galaxies as in the previous section. Fortunately, recent work on gas-dominated galaxies (Begum et al. 2008; Swaters et al. 2009; Stark et al. 2009; Trachternach et al. 2009) has made it possible to obtain an absolute calibration of the mass scale of the BTFR that is effectively independent of stellar mass estimates (McGaugh 2012).

The ideal situation would be a calibration of the BTFR with galaxies made purely of gas. In practice, this is impossible. Nevertheless, it is possible to select galaxies that are sufficiently gas-rich that the error in the stellar mass becomes a minor contributor to the error budget. This occurs when $M_g > M_*$ (McGaugh 2011).

McGaugh (2012) discusses fits to the BTFR for several distinct samples of gas-rich galaxies. Combined, these are consistent with the BTFR

$$\log M_b = 1.67 + 4 \log V_f. \quad (6)$$

In order to estimate the stellar mass, we assume that star-dominated galaxies exactly follow Equation (6). This seems like a reasonable assumption given the results of the previous section. However, the gas-rich galaxies fit by McGaugh (2012) are much slower rotators than the sample of objects here (Figure 6). It is therefore a big extrapolation to apply Equation (6) to the bright galaxies in Table 1.

We first use the measured rotation velocity and Equation (6) to estimate the total baryonic mass. The stellar mass then follows by subtracting the gas mass:

$$M_* = M_b - M_g. \quad (7)$$

The results of this computation are reported in Table 3. The first column of Table 3 gives the name of each galaxy, as in Table 1. Column 2 gives the stellar mass as estimated by the [3.6] luminosity assuming $\Upsilon_*^{[3.6]} = 0.47\ M_\odot/L_\odot$. This is provided for direct comparison to the stellar mass estimated with Equation (7), which is given in column 3. The formal uncertainty in the stellar mass is estimated by propagating the uncertainty in V_f, distance, and the gas-rich BTFR calibration. The corresponding mass-to-light ratios in the V, I, and [3.6] bands are given in columns 4–6.

Estimating stellar masses and mass-to-light ratios with this procedure is very demanding on data quality. Starting from V_f, which is typically of the order of $\sim$100 km s^{-1}, we first raise this number to a high power. We then multiply by an empirically determined constant of the same order. This gives a large number appropriate to the baryonic mass of a galaxy. We then subtract another large number, the gas mass. This procedure invites the propagation of errors. The stellar masses we obtain are nevertheless quite reasonable (Table 3). We should, however, not be surprised if this method sometimes returns unphysical results, like negative stellar masses.

Indeed, negative stellar masses are inferred four times, in DDO 168, D500-2, NGC 2366, and IC 2574. These four galaxies are the points that lie slightly above the line in Figure 2. In no case is the stellar mass significantly negative: all four are within 1σ of being positive.

The opposite situation also happens. DDO 154 is inferred to have an unreasonably large mass-to-light ratio—it is the lowest point in Figure 2. However, its stellar mass is non-zero by less than 2σ, so its large inferred mass-to-light ratio is not meaningful.

The few extremal cases are an indication of the success of the procedure. If we attempt the same exercise using line-widths instead of resolved rotation curves, we routinely find negative masses. We often also find super-maximal mass-to-light ratios, which do not occur in Table 3. The lower scatter in the BTFR obtained with resolved rotation curves is essential to the method.

One should nevertheless treat the results for individual galaxies with caution. The data are statistically indicative, but it is very hard to have confidence in any one stellar mass. Given the large extrapolation from the gas-rich regime, the stellar mass of the brightest galaxies is extremely sensitive to the slope of the BTFR (see Section 6.5).

We can check the inferred mass-to-light ratios against the expectations of population synthesis models. This is done in Figure 3, where we show the mass-to-light ratios from Table 3 as a function of color. Figure 4 shows histograms of the BTFR mass-to-light ratios.

The mass-to-light ratios estimated from the BTFR are consistent in amplitude with that expected from population synthesis. This was not guaranteed: the BTFR calibrated by gas-rich galaxies provides a constraint that is independent from the population models. While it was clear already from Figure 1 that this would follow, it need not have. Indeed, it would not have if we employed a model much different from that of Equation (3), of which there are many examples in the literature.

Nevertheless, the amplitude, slope, and scatter in Υ_* expected form population synthesis are consistent with the gas-rich BTFR. While the data are consistent with the CMLR determined photometrically, they are not precise enough to further constrain it. That is, we cannot use these data to measure the color slopes of the CMLR.

Indeed, Figure 3 does not show a strong dependence of Υ_* on color. As expected, the dependence of Υ_* on $B-V$ becomes weaker as one goes from optical to NIR. There is no hint of a slope at all at [3.6]. As expected from a population perspective, the NIR Υ_* from the BTFR is effectively constant.

If the dependence of Υ_* on $B-V$ is weak, it is virtually non-existent for the other colors. There is a hint in the data that Υ_*^V might become larger for very red $V-I$. Otherwise, Υ_* does not appear to be particularly sensitive to either $V-I$ or $J-K$. This is not surprising. It was already clear from the photometry (McGaugh & Schombert 2014) that $B-V$ contained most of the information about Υ_*, with $V-I$ carrying only a small additional amount beyond that. There is no useful information about Υ_* in $J-K$ (see also Schombert & McGaugh 2014a).

The histogram of Υ_* (Figure 4) shows scatter about a typical value. The widths of the histograms basically reflect the propagation of errors: the data are consistent with a narrow intrinsic scatter (Section 3.5). Nevertheless, it is worth noting that there is a clear and well-defined peak at a preferred value in the NIR: $\Upsilon_* = 0.45\ M_\odot/L_\odot$.

The top row of Figure 4 shows the raw distribution of Υ_*, and does not consider the expected variation with color. Since there is no expected variation with color in [3.6], the peak is clearer there than it can be in either V or I. In the bottom row of

Table 3
Stellar Masses and Mass-to-light Ratios from the BTFR

Galaxy	$M_*[3.6]$[a]	M_*(BTFR)	Υ_*^V	Υ_*^I	$\Upsilon_*^{[3.6]}$
		($10^9\ M_\odot$)		($M_\odot/L_\odot$)	
DDO 154	0.0341	0.248 ± 0.142	4.81 ± 2.76	8.44 ± 4.84	3.42 ± 1.96
D631-7	0.0458	0.156 ± 0.147	2.89 ± 2.72	3.48 ± 3.27	1.60 ± 1.51
DDO 168	0.0881	−0.0431 ± 0.0866	−0.26 ± 0.53	...	−0.23 ± 0.46
D500-2	0.186	−0.158 ± 0.413	−0.52 ± 1.35	-0.70 ± 1.83	−0.40 ± 1.05
NGC 2366	0.336	−0.365 ± 0.419	−0.80 ± 0.92	−0.99 ± 1.13	−0.51 ± 0.58
IC 2574	1.10	−0.373 ± 0.435	−0.36 ± 0.42	−0.39 ± 0.46	−0.16 ± 0.19
F563-1	1.34	2.36 ± 2.73	2.09 ± 2.42	1.89 ± 2.19	0.83 ± 0.95
NGC 2976	1.50	2.23 ± 0.53	1.98 ± 0.47	2.13 ± 0.51	0.70 ± 0.16
F568V-1	1.97	5.71 ± 3.85	2.42 ± 1.64	2.54 ± 1.71	1.36 ± 0.92
NGC 1003	2.78	0.41 ± 1.12	0.15 ± 0.40	...	0.07 ± 0.20
F568-1	3.33	2.98 ± 3.13	0.96 ± 1.01	1.00 ± 1.06	0.42 ± 0.44
NGC 7793	3.55	5.59 ± 1.43	1.87 ± 0.48	3.10 ± 0.79	0.74 ± 0.19
UGC 128	5.30	4.62 ± 4.58	1.03 ± 1.02	1.10 ± 1.09	0.41 ± 0.41
NGC 2403	5.71	11.9 ± 2.8	3.08 ± 0.72	2.38 ± 0.55	0.98 ± 0.23
NGC 925	7.42	1.42 ± 2.00	0.17 ± 0.24	0.17 ± 0.24	0.09 ± 0.12
NGC 3198	14.7	21.2 ± 3.9	1.71 ± 0.32	1.34 ± 0.25	0.68 ± 0.13
NGC 3621	15.5	6.61 ± 3.86	0.98 ± 0.57	0.93 ± 0.54	0.20 ± 0.12
NGC 3521	42.8	55.6 ± 24.8	3.57 ± 1.59	2.40 ± 1.07	0.61 ± 0.22
NGC 3031	49.6	62.3 ± 22.5	2.70 ± 0.97	1.61 ± 0.58	0.59 ± 0.26
NGC 5055	63.5	37.8 ± 14.8	1.44 ± 0.56	0.94 ± 0.37	0.28 ± 0.11
NGC 2998	75.0	47.9 ± 13.0	0.64 ± 0.17	...	0.30 ± 0.08
NGC 6674	108.	94.1 ± 22.9	1.49 ± 0.36	...	0.41 ± 0.10
NGC 7331	122.	153. ± 32.	4.00 ± 0.84	2.28 ± 0.47	0.59 ± 0.12
NGC 801	126.	42.9 ± 15.4	0.60 ± 0.21	...	0.16 ± 0.06
NGC 5533	142.	106. ± 24.	1.69 ± 0.38	...	0.35 ± 0.08
UGC 2885	220.	304. ± 69.	1.70 ± 0.38	...	0.65 ± 0.15

[a] Stellar masses assuming $\Upsilon_*^{[3.6]} = 0.47\ M_\odot/L_\odot$ are included for comparison.

Figure 4, we show the histogram of Υ_* relative to that expected from Equation (3). Here it can be seen that the data do peak near the value expected from population synthesis: there is value in the color informed Υ_* estimate of the CMLR.

An obvious consequence is that the luminosity in any band is a good approximation of the stellar mass. This approximation can be improved with use of color information. The amount of improvement is limited by the intrinsic scatter in the CMLR. Both the scatter and the color term are minimized in the NIR. This makes the NIR luminosity the best available proxy for stellar mass.

The results here are consistent with the results of Section 3.5. The stellar population estimate of the BTFR gives a relation indistinguishable from the separate gas-rich calibration. It makes little difference which method we choose. Either the data fall exactly on the BTFR and give the scatter seen in Figure 3, or the galaxies follow exactly this lines of Equation (3) in Figure 3 with the scatter seen in Figure 1. There has to be some scatter in Υ_*, leaving precious little room for intrinsic scatter in the BTFR.

It remains unclear why the BTFR is so well posed as a relation between baryonic mass and the flat rotation velocity. It does not follow from structure formation simulations without further assumptions. It has become common to invoke feedback from star formation in this context (e.g., Governato et al. 2007; Dutton 2012), but it is hard to see how the chaotic processes of supernovae returning energy to the ISM can result in the negligible scatter observed in the BTFR. The only theory to anticipate the specific M_b–V_f relation that we observe is MOND (Milgrom 1983).

Regardless of the physics underlying the BTFR, it is of enormous utility to have such a relation. We emphasize that the BTFR constructed here is empirical, making no reference to either dark matter or MOND. It relies only on observational data and stellar population synthesis models to inform the CMLR.

5. A CONSTRAINT ON THE IMF

Returning to the matter of stellar mass, there is additional information in the BTFR. The normalization of the BTFR calibrated by gas-rich galaxies is effectively independent of stellar mass estimates. In contrast, the population synthesis mass estimates are very sensitive to the IMF. That the two are consistent implies that we are not far wrong about the IMF. Nevertheless, we can query the data to see what mass-to-light ratio is preferred. Rather than take the population synthesis mass at face value and fit the BTFR, we adjust the stellar mass of bright galaxies to find the best agreement with the BTFR previously fit to gas-rich galaxies. This leads to a constraint on the IMF (Stark et al. 2009).

In order to find the ideal match with the BTFR, we adjust the zero point in Equation (3) while holding the color slope fixed. We then find the zero point that best matches the BTFR of McGaugh (2012). That is, we determine the value Δa in

$$\log \Upsilon_* = a + b(B - V) + \Delta a \quad (8)$$

that best matches the gas-rich BTFR.

The net effect of this exercise is a small shift of the intercept in each band. The result is $\Delta a = -0.015$ in V, +0.06 in I, and

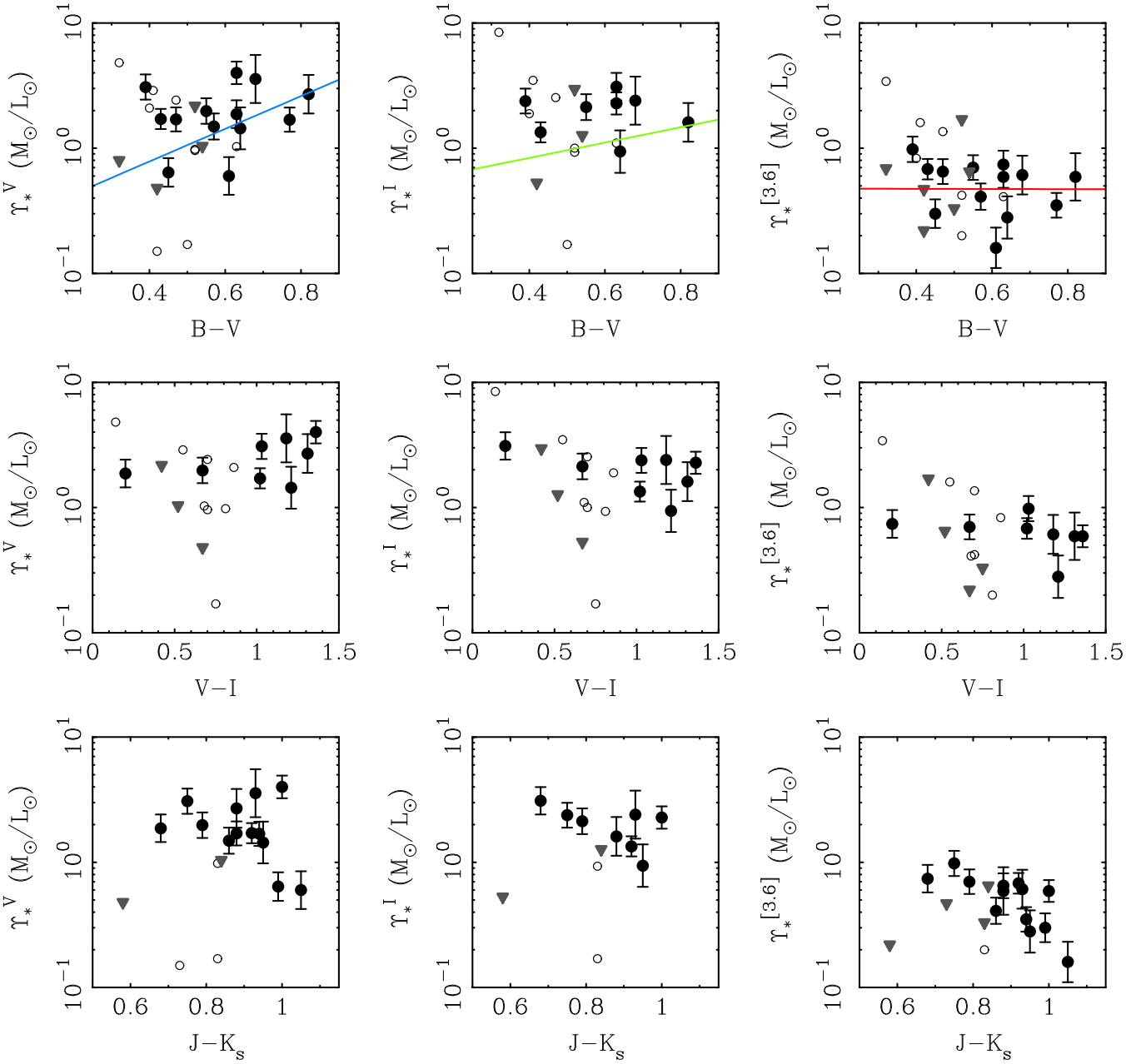

Figure 3. Stellar mass-to-light ratios (Table 3) inferred from the gas-rich calibration of the BTFR. Mass-to-light ratios in V (left column), I (middle column), and [3.6] (right column) are plotted as a function of color in $B-V$ (top row), $V-I$ (middle row), and $J-K_s$ (bottom row). Data with uncertainties in stellar mass <50% are shown as solid points. Less accurate data are shown as open circles. Galaxies with formally negative stellar masses are shown as 2σ upper limits (gray triangles). The mass-to-light ratios predicted by Equation (3) are shown as lines in the panels of the top row.

−0.019 in [3.6]. This is what it takes to make the dashed lines in the bottom row of Figure 1 fall on top of the solid lines.

These shifted zero points are not significantly different from the original population synthesis values. For example, the NIR value changes from $\Upsilon_*^{[3.6]} = 0.47$ to 0.45 $M_\odot/L_\odot$. Similarly, in the galaxies for which we have K-band data, the mean shifts from $\Upsilon_*^K = 0.60$ to 0.57 $M_\odot/L_\odot$ ($\Delta a = -0.022$). This corresponds to a ratio $\Upsilon_*^K/\Upsilon_*^{[3.6]} = 1.27$, consistent with the 1.29 we estimated photometrically (McGaugh & Schombert 2014).

This nice consistency may seem mundane, but is actually a rather important observation. That Δa is small implies that the population models are nearly correct, provided they adopt the right IMF. The data are consistent with a Kroupa or Chabrier IMF. The Salpeter IMF, as usually employed, is a bit too heavy (see discussion in Stark et al. 2009). This is consistent with what we know about the IMF locally, in which the numbers of low-mass stars does not continue to increase as a Salpeter power law (Kroupa 1998; Chabrier 2003).

6. COMPARISON TO OTHER METHODS

The absolute calibration of stellar mass is of obvious interest. In this section, we compare the normalization found from the BTFR to other methods in the literature. A largely consistent picture emerges, with one important exception.

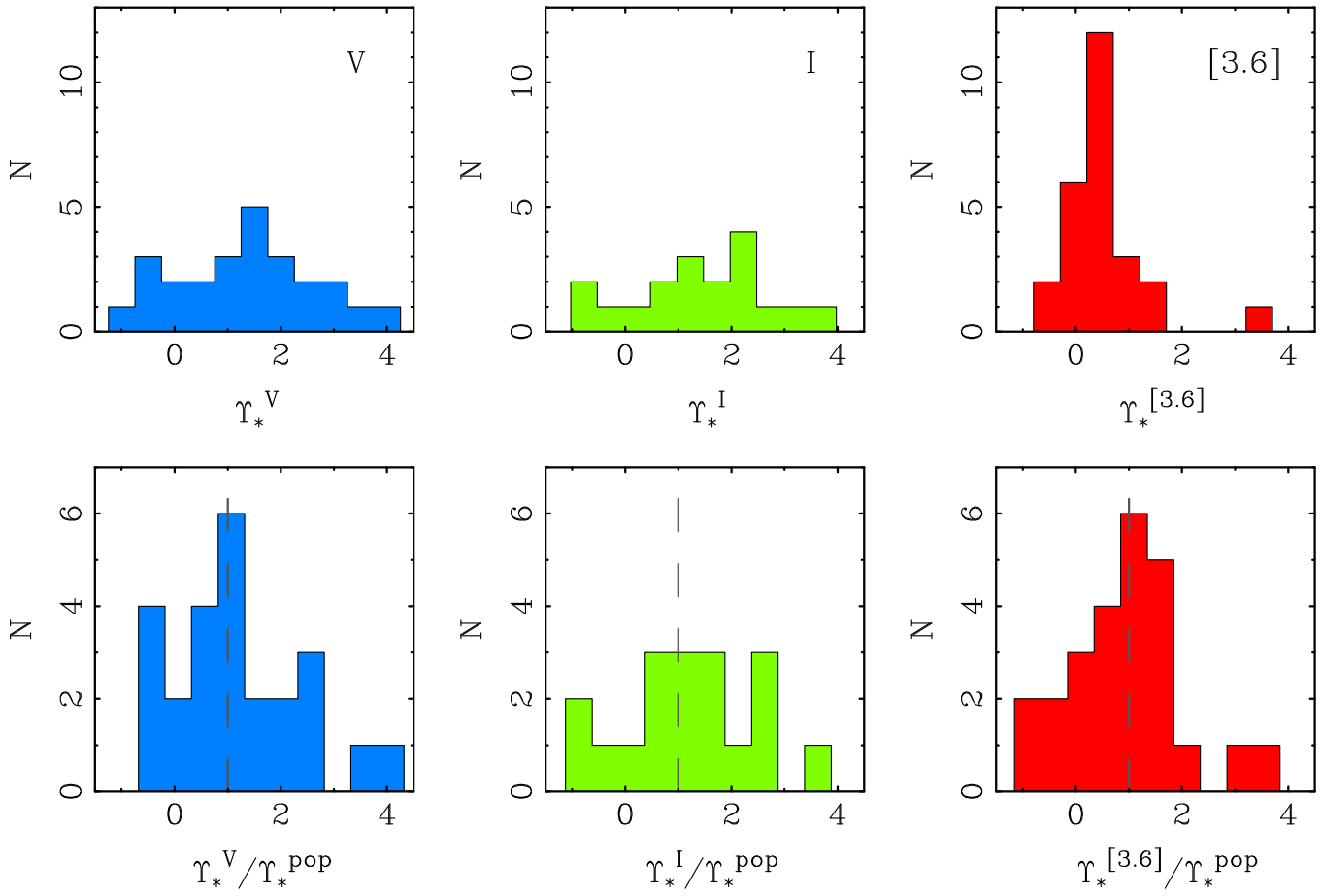

Figure 4. Histograms of stellar mass-to-light ratios inferred from the BTFR in V (left column), I (middle column), and [3.6] (right column). The top row shows the measured mass-to-light ratios while the bottom row shows Υ_* relative to the population synthesis expectation of Equation (3) (dashed lines). The bin size and plot scale are the same for all filters within each row. The data are consistent with $\Upsilon_*^{[3.6]} = 0.45\ M_\odot/L_\odot$ with modest intrinsic scatter.

Table 4
Mass-to-Light Ratio Estimates

Calibration	Method	$\langle\Upsilon_*^V\rangle$	$\langle\Upsilon_*^I\rangle$	$\langle\Upsilon_*^K\rangle$	$\langle\Upsilon_*^{[3.6]}\rangle$	References
Gas Rich	BTFR	1.38	1.42	0.57	0.45	1
DiskMass[a]	Vertical σ_z	0.74	0.65	0.31	0.24	2
DiskMass[a]	DM-adjusted	0.57	0.50	0.24	0.19	3
Milky Way	Star counts	1.5	1.2	...	...	4
Milky Way	Terminal v_t	1.53	1.22	0.63	0.49	5
Milky Way	Vertical K_z	1.64	1.31	0.66	0.51	6
LMC	Star counts	...	...	0.65	0.5	7
Bell	Popsynth	1.43	1.25	0.73	0.62	8
Portinari	Popsynth	1.32	1.11	0.50	0.41	9
Zibetti	Popsynth[b]	1.07	0.76	0.21	0.14	10
Into	Popsynth[b]	1.19	0.99	0.41	0.33	11
Equation (3)	Popsynth	1.43	1.24	0.60	0.47	12
Schombert	Popsynth	⋯	⋯	0.65	0.5	13
Meidt	Popsynth	⋯	⋯	0.77	0.6	14

Refrences (1) This work, (2) Martinsson et al. (2013a), (3) Swaters et al. (2014), (4) McGaugh (2008), (5) Flynn et al. (2006), (6) Bovy & Rix (2013), (7) Eskew et al. (2012), (8) Bell et al. (2003), (9) Portinari et al. (2004), (10) Zibetti et al. (2009), (11) Into & Portinari (2013), (12) McGaugh & Schombert (2014), (13) Schombert & McGaugh (2014a), (14) Meidt et al. (2014).

Notes. Color-dependent population synthesis models are evaluated at $B-V = 0.6$. To compare the K_s and [3.6] bands we assume $\Upsilon_*^K = 1.29\Upsilon_*^{[3.6]}$ (McGaugh & Schombert 2014), with the exception of the BTFR method which independently suggests $\Upsilon_*^K = 1.27\Upsilon_*^{[3.6]}$ (see text).

[a] For comparison with other methods, the V and I-band values are approximated by scaling from the K-band measurement with Equation (3).

[b] These models do not give self-consistent stellar masses unless the NIR mass-to-light ratio is adjusted to larger values: $\Upsilon_*^K \approx 0.58$ and $\Upsilon_*^{[3.6]} \approx 0.45\ M_\odot/L_\odot$ (see discussion in McGaugh & Schombert 2014).

Table 4 summarizes various estimates of the stellar mass-to-light ratios of disk galaxy stellar populations. Column 1 gives a name for each method considered as described in column 2. Columns 3–6 give typical mass-to-light ratios in the *V*, *I*, *K*, and [3.6] bands. We include the *K*-band here for comparison with [3.6]. These two bands are nearly interchangeable photometrically (Schombert & McGaugh 2014a, 2014b). We convert between them assuming the ratio of mass-to-light ratios is constant so that results limited to one or the other band can be directly compared. Column 8 gives the reference for each Υ_* calibration.

Our result from Section 4 is given first. These are consistent with our previous attempt to employ this method (Stark et al. 2009). It is also consistent with many, but not all, population synthesis estimates. The NIR Υ_* are hardly different from Equation (3). The tweak in the *V*-band is also negligible, but that in the *I*-band is more noticeable. These are sensitive to color, and are estimated at $B-V=0.6$ to provide a uniform comparison. We do not consider the difference between the BTFR $\Upsilon_*^I \approx 1.4\ M_\odot/L_\odot$ and the value from Equation (3) of $\Upsilon_*^I \approx 1.2\ M_\odot/L_\odot$ to be particularly significant. It perhaps serves more as an illustration of just how sensitive the method is, as this is the shift ($\Delta a = 0.06$) required to match the two nearly indistinguishable lines in the bottom middle panel of Figure 1. Indeed, the positive Δa in the *I*-band (when the other filters are slightly negative) may simply be the result of missing data in that filter for some of the brighter galaxies.

6.1. The DiskMass Survey

One of the most important works constraining the stellar masses of disk galaxies is the DiskMass survey (Bershady et al. 2010, 2011). DiskMass observes velocity dispersions across the disks of face-on galaxies. It then assumes a disk thickness that is statistically consistent with observations of edge-on galaxies (Kregel et al. 2005) in order to estimate the stellar mass profile. This method measures the vertical restoring force to the disk, and is independent of the IMF.

The results of the DiskMass survey are summarized in the second and third rows. Martinsson et al. (2013a) found a near-constant NIR mass-to-light ratio of $\langle\Upsilon_*^K\rangle = 0.31 \pm 0.07\ M_\odot/L_\odot$. The small scatter and near-constancy of the mass-to-light ratio is consistent with our findings here. The normalization differs by nearly a factor of two.

The rather sub-maximal disks found by the DiskMass survey imply that the dark matter halo contributes a non-negligible amount to the observed velocity dispersions. This will inevitably drive the implied mass of the disk down further. Swaters et al. (2014) make a first estimate of this effect, revising the mean mass-to-light ratio down to $\langle\Upsilon_*^K\rangle = 0.24\ M_\odot/L_\odot$. This is a factor of ∼2.4 times lower than what we find here. The effect of the dark matter halos may be compensated somewhat by the presence of super-thin disks in some galaxies (Schechtman-Rook & Bershady 2014). We will return to the factor of ∼2 discrepancy between the DiskMass and BTFR results after discussing other constraints.

6.2. The Milky Way

Our own Milky Way provides a unique environment in which we can hope to both count stars directly and constrain their mass from kinematics. This is a rich field that is rapidly becoming richer; we consider here only a few relevant results. Flynn et al. (2006) use star counts from two independent surveys to constrain Galactic structure. Among other things, they estimate the mass-to-light ratio of the stellar disk of the Milky Way to be $\Upsilon_*^V = 1.5 \pm 0.2$ and $\Upsilon_*^I = 1.2 \pm 0.2\ M_\odot/L_\odot$.

Starting from an initially exponential disk, McGaugh (2008) deformed the radial mass distribution of the Galactic disk in order to fit the terminal velocity curve in the fourth quadrant (Luna et al. 2006; McClure-Griffiths & Dickey 2007). The result is a mass model with bumps and wiggles reminiscent of those observed in other spirals. Indeed, the Centaurus arm is prominent in the inferred Milky Way mass profile. Matching the details of the terminal velocity curve requires the disk to be nearly maximal. The stellar mass obtained in this way is ∼2% greater than estimated by Flynn et al. (2006): $M_* = 5.48 \times 10^{10}\ M_\odot$ for $R_0 = 8$ kpc. To estimate the mass-to-light ratio, we adopt the total *I*-band luminosity estimated by Flynn et al. (2006), $L_I = 4.5 \times 10^{10}\ L_\odot$, and the *K*-band luminosity from Drimmel & Spergel (2001), $L_K = 8.6 \times 10^{10}\ L_\odot$, which includes a somewhat uncertain correction for the bulge fraction. The result is $\Upsilon_*^I = 1.22\ M_\odot/L_\odot$ and $\Upsilon_*^K = 0.63\ M_\odot/L_\odot$.

Bovy & Rix (2013) have measured the vertical restoring force to the disk $K_z(|Z| < 1.1$ kpc) over a wide range of Galactocentric radii. They obtain a mass for the stellar disk of $M_* = 4.6 \pm 0.3 \times 10^{10}\ M_\odot$. Combining this with the disk-only luminosity estimated by Flynn et al. (2006), $L_I^{\rm disk} = 3.5 \times 10^{10}\ L_\odot$, and $L_K^{\rm disk} = 6.9 \times 10^{10}\ L_\odot$ from Drimmel & Spergel (2001) yields $\Upsilon_*^I = 1.31 \pm 0.09\ M_\odot/L_\odot$ and $\Upsilon_*^K = 0.66 \pm 0.04\ M_\odot/L_\odot$. The bulge component is excluded from this calculation, as the measurement of Bovy & Rix (2013) is specific to the Galactic disk. The uncertainty in the mass-to-light ratio here is only that from the error in stellar mass quoted by Bovy & Rix (2013), and does not include the uncertainty in the luminosity. The latter translates to roughly ±0.2 in Υ_* in absolute terms.

The three independent methods just discussed, star counts, the radial force in the disk, and the vertical force from the disk, all find mass-to-light ratios for the Milky Way that are consistent within the errors. They are also consistent with the result from the BTFR. They are not consistent with the low mass-to-light ratios implied by DiskMass, despite the similarity of the DiskMass approach to that of Bovy & Rix (2013).

6.3. The LMC

Eskew et al. (2012) perform star counts in the LMC with NIR data. They sum up the mass of the stars observed to find $\Upsilon_*^{[3.6]} = 0.5\ M_\odot/L_\odot$. This method depends some on the IMF, as one does have to extrapolate to unseen, low-mass stars. As in the Milky Way, the stars are counted directly, albeit to a brighter limit, so the assumption on the IMF is less strong than in population synthesis models.

6.4. Population Synthesis

Stellar population synthesis is a well-developed field. It is possible to use our knowledge of stellar evolution to construct detailed models for the composite stellar populations of spiral galaxies for various assumed star formation histories and metallicities (e.g., Bruzual & Charlot 2003; Le Borgne

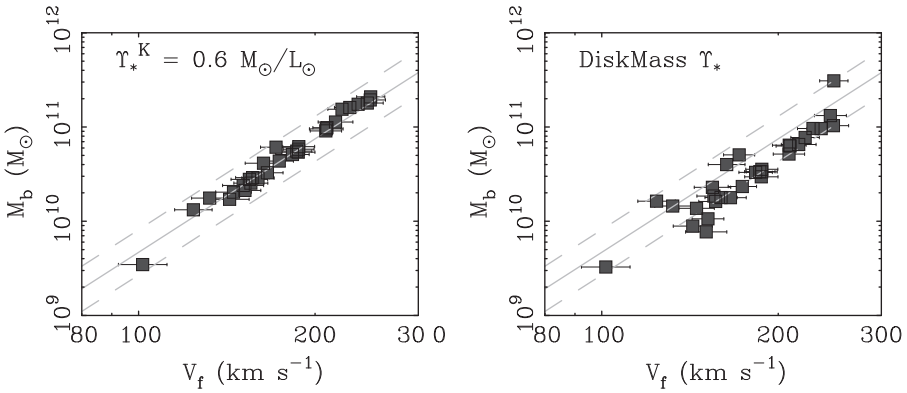

Figure 5. BTFR constructed from the galaxies in the DiskMass survey (Bershady et al. 2010). Both panels are identical along the abscissa, with V_f from Martinsson et al. (2013b). They differ in stellar mass along the ordinate. The left panel shows the baryonic mass for stellar masses with a constant K-band mass-to-light ratio from population models ($\Upsilon_*^K = 0.6\ M_\odot/L_\odot$: McGaugh & Schombert 2014) plus the gas masses tabulated by Martinsson et al. (2013a). The right panel uses the same gas masses, but adopts the stellar masses found by Martinsson et al. (2013a). The BTFR calibration of the gas-rich galaxies (McGaugh 2012) is shown as a solid line in both panels, with its 1σ uncertainty as dashed lines.

et al. 2004). For an assumed IMF, such models can be used to estimate the mass-to-light ratio of a population.

One expects that as stars age, the population will redden and the mass-to-light ratio will increase. Many models have been constructed to quantify this behavior. A few relevant ones are noted in Table 4.

The models of Bell et al. (2003), Portinari et al. (2004), Zibetti et al. (2009), and Into & Portinari (2013) have been explored in detail by McGaugh & Schombert (2014). These all give comparable mass-to-light ratios in the optical portion of the spectrum: $1 < \Upsilon_*^V < 1.5\ M_\odot/L_\odot$ evaluated at $B - V = 0.6$. Small differences there appear to be attributable largely to modest differences in the assumed IMF. However, the models have very different SEDs in the NIR, where agreement breaks down. In terms of Υ_*, Bell et al. (2003) estimate $\Upsilon_*^K = 0.73\ M_\odot/L_\odot$ for $B - V = 0.6$ while Zibetti et al. (2009) give $\Upsilon_*^K = 0.21\ M_\odot/L_\odot$. This large discrepancy persists if we correct for difference in the IMF: scaling up the Zibetti et al. (2009) estimate to match that of Bell et al. (2003) in the V-band has little impact in the NIR: $\Upsilon_*^K = 0.21 \rightarrow 0.28\ M_\odot/L_\odot$. This is still a factor of 2.6 lower than the $0.73\ M_\odot/L_\odot$ of Bell et al. (2003). The models do not produce consistent SEDs (Kriek et al. 2010).

McGaugh & Schombert (2014) used multi-wavelength photometric data to test these various models. Requiring self-consistency—i.e., that the same mass of stars produce the observed luminosity in each band for every galaxy—leads to Equation (3). This stipulation obliges all models to fall in the range $0.4 < \Upsilon_*^{[3.6]} < 0.5\ M_\odot/L_\odot$.

The reasons for the difference between models are many, but the primary issue appears to be the treatment of thermally pulsing AGB (TP-AGB) stars. The luminosity of this component is grossly exaggerated in the models of Zibetti et al. (2009). The TP-AGB stars, as modeled, produce a lot of NIR photons without contributing much in the optical nor representing much stellar mass. Consequently, the NIR mass-to-light ratios are underestimated. A similar conclusion was reached by Zibetti et al. (2013), who sought but did not find the predicted spectral features of TP-AGB stars.

We constructed our own population models in Schombert & McGaugh (2014a). These models have an empirically motivated distribution of stellar metallicities as well as different ages corresponding to a variety of star formation histories. The metallicity distribution weakens the dependence of the NIR mass-to-light ratio on color relative to models built with a single metallicity. Most of model parameter space is consistent with $\Upsilon_*^{[3.6]} = 0.5\ M_\odot/L_\odot$. Independently, Meidt et al. (2014) obtain $\Upsilon_*^{[3.6]} = 0.6\ M_\odot/L_\odot$ albeit with a stronger color dependence. These values are consistent with the majority of methods. The exception to this is the DiskMass result, which we examine further in the next section.

6.5. The DiskMass BTFR

Examination of Table 4 suggests that nearly all methods are consistent with a NIR mass-to-light ratio $\Upsilon_*^K \approx 0.57$ and $\Upsilon_*^{[3.6]} \approx 0.45\ M_\odot/L_\odot$. Since the population synthesis result for a Kroupa IMF is consistent with the normalization independently required by the gas-rich BTFR, it is tempting to conclude that the problem of stellar mass in disk galaxies is essentially solved. Unfortunately, the method of vertical velocity dispersions, as employed by the DiskMass project (Bershady et al. 2010, 2011), does not yield a consistent result.

Since DiskMass provides a result that is independent of the IMF, it deserves more consideration than the mutual consistency of the various population synthesis models. We can maintain that consistency while rescaling the IMF to match the DiskMass scale with the translation $\Delta a = -0.29$. So conceivably we simply need to adopt a different IMF in the population modeling. While this may be acceptable form a population synthesis perspective, it is harder to reconcile with Milky Way constraints. We check here whether we can reconcile it with the BTFR.

We construct the BTFR from the DiskMass data (Martinsson et al. 2013a, 2013b) for two choices of mass-to-light ratio. In one case, we use that measured by DiskMass (Martinsson et al. 2013a). In the other, we adopt a constant mass-to-light ratio $\Upsilon_*^K = 0.6\ M_\odot/L_\odot$ as suggested by population synthesis models (McGaugh & Schombert 2014). The result is shown in Figure 5. Unsurprisingly, the two BTFR are shifted with respect to each other due to the difference in the adopted mass-to-light ratios.

The BTFR constructed using the population synthesis value $\Upsilon_*^K = 0.6\ M_\odot/L_\odot$ places the DiskMass galaxies directly on the BTFR fit independently to gas-rich galaxies by McGaugh

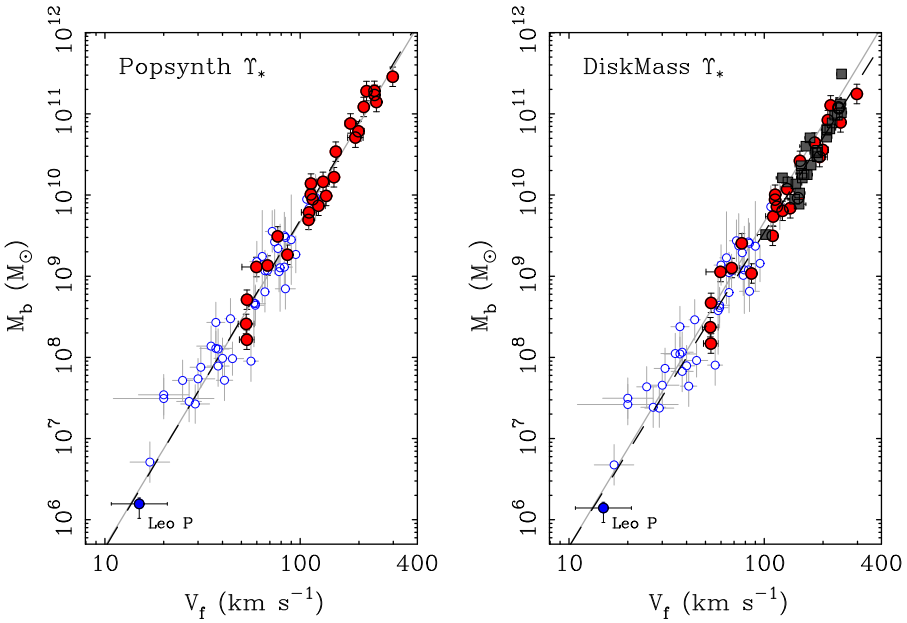

Figure 6. BTFR from the [3.6] sample (solid red circles) compared to the gas-rich galaxy sample of McGaugh (2012, open circles) and the DiskMass data (squares). The recently discovered, very low-mass dwarf galaxy Leo P (Giovanelli et al. 2013; Rhode et al. 2013) is also shown. In the left panel, the [3.6] data are shown with the population synthesis mass-to-light ratio $\Upsilon_*^{[3.6]} = 0.47\ M_\odot/L_\odot$ and 0.12 dex uncertainty. In the right panel, the DiskMass data are shown as in Figure 5. The stellar masses of the other two data sets are scaled down to match the DiskMass scale ($\Upsilon_*^{[3.6]} = 0.24\ M_\odot/L_\odot$ for the [3.6] data). This makes little difference to the gas-rich sample, but the [3.6] sample shifts to match the DiskMass data. The solid line in both panels is the fit to the gas-rich data alone from McGaugh (2012). A fit to the combined gas-rich plus [3.6] sample is shown as the dashed line in the left panel. In the right panel, the dashed line is a fit to the gas-rich plus DiskMass sample. A tiny adjustment in slope (see Table 5) over the six decades in mass illustrated here suffices to accommodate the DiskMass data with the gas-rich data.

Table 5
BTFR of Combined Samples

Sample	x	$\log A$
3.6 + gas-rich	4.04 ± 0.09	1.61 ± 0.18
DiskMass + gas	3.87 ± 0.10	1.80 ± 0.21

Note. Fits of the form $\log M_b = \log A + x \log V_f$.

(2012). This is not guaranteed to happen. The gas-rich galaxies are, by and large, much slower rotators than the bright spirals of the DiskMass sample. The extrapolation of that fit will not work if the mass-to-light ratio is discordant.

Indeed, the data for the mass-to-light ratios determined by DiskMass are systematically shifted off the gas-rich BTFR. Most of the data parallel it, falling $\sim 1\sigma$ below the fit line. The DiskMass data are consistent with a slope four BTFR, but with a lower normalization. One possibility is thus that the DiskMass Υ_* are too low due to some unknown systematic error, and simply need to be shifted upwards to be consistent with other results.

Looking closely at the DiskMass BTFR (right panel of Figure 5), one may note that the data almost bifurcate into two parallel relations. Most of the data fall low, but a half-dozen galaxies stand to one side, consistent with the gas-rich BTFR. We do not know why the data might split like this, and suspect it may be indicative of a systematic error. This bifurcation disappears when a higher, constant K-band mass-to-light ratio is adopted. The scatter also decreases, but this is an inevitable result of setting the inclinations of the DiskMass galaxies with the K-band LTFR in the first place (Martinsson et al. 2013a). As Υ_* grows, the gas becomes less important to M_b, and one eventually just recovers a scaled version of the LTFR.

So far, we have kept distinct the various samples: gas-rich galaxies, the [3.6] sample of this paper, and the DiskMass data. Another approach is to make a fit of the BTFR with the combined data. The [3.6] and DiskMass data are consistent with each other for the same choice of mass-to-light ratio, so we make two combined fits. In one, we simply combine the [3.6] data as presented here with the gas-rich data from McGaugh (2012). In the other, we combine the DiskMass data with the gas-rich data, scaling the stellar masses of the gas-rich galaxies down by a factor of two to be consistent with the DiskMass scale. These fits are shown in Figure 6 with fit parameters given in Table 5.

In combining the [3.6] and gas-rich samples, we have been careful to exclude duplicate galaxies. The gas-rich galaxies from McGaugh (2012) are largely independent of the sample here, but there is some overlap. Of the 47 galaxies considered in McGaugh (2012) and the 26 in Table 1, there are 7 objects in common: D631-7, DDO 168, IC 2574, F568-V1, F568-1, NGC 2403, and NGC 3198. These seven are plotted (and fit) only once in Figure 6, as part of the [3.6] sample.

The combined fit obtained in this fashion is consistent with the previous fit to the gas-rich data alone. It is slightly steeper, as we have retained the stellar population estimate of $\Upsilon_*^{[3.6]} = 0.47\ M_\odot/L_\odot$, which is ever so slightly higher than the 0.45 of a straight extrapolation from the gas-rich BTFR. The fit lines are hardly distinguishable.

Indeed, the [3.6] data follow the extrapolation of the fit to the gas-rich galaxies remarkably well. This happens with zero effort: the location of the galaxies from Table 1 in the BTFR plane is determined entirely by the data and the mass-to-light ratio provided by population modeling. It is completely independent of the gas-rich calibration.

The gas-rich BTFR calibration also extrapolates well downwards to lower masses. This holds for both star-dominated dwarf Spheroidals (McGaugh & Wolf 2010) and for the recently discovered gas-rich dwarf Leo P (Giovanelli et al. 2013). In Figure 6 we adopt the distance of McQuinn et al. (2013) when plotting the stellar (Rhode et al. 2013) and gas (Giovanelli et al. 2013) mass of Leo P so that the datum is independent of the fitted relation. Leo P falls along the extrapolation of the BTFR to lower rotation velocity just as the [3.6] data fall along the extrapolation to higher V_f. The BTFR appears to be well described as a single power law over nearly six decades in mass.

In the combined DiskMass plus gas-rich BTFR fit, the relation again appears to be well described as a single power law. The chief difference is a slightly lower slope. Instead of $x \approx 4.0$, we now find $x \approx 3.9$.

This change of slope is driven by the lower mass-to-light ratios favored by DiskMass. The lower stellar masses adopted for the gas-rich galaxies themselves make no perceptible difference. The baryonic masses of these objects were already dominated by gas; for the new assumption this is slightly more true. However, the gas-rich galaxies are predominantly slow rotators, while the DiskMass sample is composed entirely of fast rotators. In order to fit the two data sets simultaneously, the BTFR simply pivots around the low-mass end, with the fitting routine selecting the slope necessary to hit the data at the high-mass end. The two lines illustrated in the right panel of Figure 6 are indistinguishable over the range constrained by the gas-rich data, but the slight difference in their slopes amounts to a factor of ~2 in Υ_* for the fast rotators.

It therefore appears that a factor of ~2 systematic uncertainty in stellar mass persists. The natural conclusion of our work is that the population synthesis models are essentially correct for a reasonable (e.g., Kroupa) IMF. However, we cannot exclude the lower mass scale indicated by the DiskMass data. The BTFR fit to DiskMass is within the uncertainties of the original gas-rich BTFR fit.

The situation could be improved with better data. Direct distance measurements of many gas-rich galaxies would considerably improve the calibration. If the small intrinsic scatter of the BTFR persists, then the scatter will come down as the data improve. The gas-rich BTFR provides a promising new method to constrain the absolute stellar mass scale.

7. CONCLUSIONS

We have weighed stellar disks in two distinct ways. We have used a traditional population synthesis approach with updated color–mass-to-light ratio relations (CMLR; McGaugh & Schombert 2014). Separately, we have inferred the stellar mass required for bright galaxies to lie along the BTFR calibrated by gas-rich galaxies. These independent approaches yield consistent results.

We construct Tully–Fisher relations in the V, I, and [3.6] bands together with measurements of the outer, flat rotation velocity from well resolved 21 cm data cubes. Each band gives a distinct LTFR. Each LTFR has a different slope, intercept, and scatter.

The CMLR obtained by requiring photometric self-consistency by McGaugh & Schombert (2014) successfully converts the different LTFR into a consistent STFR. This provides kinematic confirmation of the photometric results. The slopes of the CMLR obtained by McGaugh & Schombert (2014) must be approximately correct, or self-consistent STFR would not follow.

We use the scatter about the STFR to estimate the intrinsic scatter in the CMLR. The scatter in stellar mass is 0.16 dex in V, 0.13 in I, and 0.12 in [3.6]. The trend for smaller scatter toward redder wavelengths follows the expectation of stellar population models. Indeed, the modest amount of scatter in the NIR is consistent with the models of Bell & de Jong (2001) and Portinari et al. (2004), who estimate 0.1 and 0.15 dex in the K-band, respectively. This consistency implies that the variation in star formation history from galaxy to galaxy suffices to explain the observed scatter, leaving little room for other sources of scatter. This in turn implies that the IMF is effectively universal, at least when averaged over entire galaxies.

The stellar masses estimated with our CMLR also lead to nice convergence in the BTFR. The BTFR obtained in this fashion is consistent with that obtained independently from gas-rich galaxies (McGaugh 2012). The slope is steep, being very close to $x = 4$ in $M_b \propto V_f^x$. There is no indication of a bend that transitions between a steeper slope at low mass and a shallower slope at high mass as suggested by some models (e.g., Trujillo-Gomez et al. 2011).

The intrinsic scatter of the BTFR is very small, consistent with zero. Effectively all of the observed scatter can be attributed to observational uncertainties and the scatter in stellar mass-to-light ratios. Ignoring these, the upper limit on intrinsic scatter is that observed at [3.6]: 0.13 dex. This is difficult to understand in the context of dark matter models, in which there should be a considerable amount of scatter from halo to halo (Eisenstein & Loeb 1996; McGaugh & de Blok 1998; Bullock et al. 2001).

The BTFR calibrated by gas-dominated galaxies provides an independent constraint on stellar mass. This approach also yields a typical 3.6 μm mass-to-light ratio of $\Upsilon_*^{[3.6]} = 0.45\ M_\odot/L_\odot$, with a corresponding value in the K_s-band of $\Upsilon_*^K = 0.57\ M_\odot/L_\odot$. The scatter about these typical values is 0.12 dex, consistent with the anticipated variation in star formation histories (Bell & de Jong 2001; Portinari et al. 2004; Kelson 2014).

An important consequence of this result is that the NIR luminosity of a galaxy is a good proxy for its stellar mass. Workers wishing to estimate the the stellar mass of galaxies would do well to measure this quantity and adopt a constant NIR mass-to-light ratio as calibrated here. If a NIR luminosity is not available, an optical luminosity is also a good proxy, albeit with more scatter and some color dependence. Contrary to our initial hope, there appears to be little value added in fitting the entire SED of galaxies, at least so far as their mass-to-light ratio is concerned: most of the information about the mass-to-light ratio is carried by a single color like B–V. Further color-based corrections are more likely to reveal systematic uncertainties in stellar population models than they are to improve the estimate of stellar mass, at least at this juncture.

The BTFR provides a new method to calibrate the absolute scale of stellar mass in rotating galaxies. It provides a useful constraint that is consistent with stellar population synthesis models. The accuracy of this method could be considerably improved with straightforward observations, such as direct distance measurements of gas-rich galaxies.

We thank the referee, Dennis Zaritsky, for a thoughtful review that led us to broaden the scope of this paper. We also thank Matt Bershady and Rob Swaters for conversations about the DiskMass project. This work is based in part on observations made with the *Spitzer Space Telescope*, which is operated by the Jet Propulsion Laboratory, California Institute of Technology under a contract with NASA. Support for this work was provided by NASA through an award issued by JPL/Caltech. Other aspects of this work were supported in part by NASA ADAP grant NNX11AF89G. This research has made use of the NASA/IPAC Extragalactic Database (NED) which is operated by the Jet Propulsion Laboratory, California Institute of Technology, under contract with the National Aeronautics and Space Administration.

REFERENCES

Begum, A., Chengalur, J. N., Karachentsev, I. D., & Sharina, M. E. 2008, MNRAS, 386, 138
Bell, E. F., & de Jong, R. S. 2001, ApJ, 550, 212
Bell, E. F., McIntosh, D. H., Katz, N., & Weinberg, M. D. 2003, ApJS, 149, 289
Bershady, M. A., Martinsson, T. P. K., Verheijen, M. A. W., et al. 2011, ApJL, 739, L47
Bershady, M. A., Verheijen, M. A. W., Swaters, R. A., et al. 2010, ApJ, 716, 198
Bottema, R., Pestaña, J. L. G., Rothberg, B., & Sanders, R. H. 2002, A&A, 393, 453
Bovy, J., & Rix, H.-W. 2013, ApJ, 779, 115
Bruzual, G., & Charlot, S. 2003, MNRAS, 344, 1000
Bullock, J. S., Kolatt, T. S., Sigad, Y., et al. 2001, MNRAS, 321, 559
Chabrier, G. 2003, ApJL, 586, L133
Conroy, C., & Gunn, J. E. 2010, ApJ, 712, 833
Dale, D. A., Bendo, G. J., Engelbracht, C. W., et al. 2005, ApJ, 633, 857
de Blok, W. J. G., & McGaugh, S. S. 1996, ApJL, 469, L89
de Blok, W. J. G., McGaugh, S. S., & van der Hulst, J. M. 1996, MNRAS, 283, 18
de Blok, W. J. G., Walter, F., Brinks, E., et al. 2008, AJ, 136, 2648
Drimmel, R., & Spergel, D. N. 2001, ApJ, 556, 181
Dutton, A. A. 2012, MNRAS, 424, 3123
Eisenstein, D. J., & Loeb, A. 1996, ApJ, 459, 432
Eskew, M., Zaritsky, D., & Meidt, S. 2012, AJ, 143, 139
Flynn, C., Holmberg, J., Portinari, L., Fuchs, B., & Jahreiß, H. 2006, MNRAS, 372, 1149
Giovanelli, R., Haynes, M. P., Adams, E. A. K., et al. 2013, AJ, 146, 15
Governato, F., Willman, B., Mayer, L., et al. 2007, MNRAS, 374, 1479
Into, T., & Portinari, L. 2013, MNRAS, 430, 2715
Kelson, D. D. 2014, arXiv:1406.5191
Kennicutt, R. C., Jr., Armus, L., Bendo, G., et al. 2003, PASP, 115, 928
Kregel, M., van der Kruit, P. C., & Freeman, K. C. 2005, MNRAS, 358, 503
Kriek, M., Labbé, I., Conroy, C., et al. 2010, ApJL, 722, L64
Kroupa, P. 1998, in ASP Conf. Ser. 134, Brown Dwarfs and Extrasolar Planets, ed. R. Rebolo, E. L. Martin, & M. R. Zapatero Osorio (San Francisco, CA: ASP), 483
Le Borgne, D., Rocca-Volmerange, B., Prugniel, P., et al. 2004, A&A, 425, 881
Leroy, A. K., Walter, F., Brinks, E., et al. 2008, AJ, 136, 2782
Luna, A., Bronfman, L., Carrasco, L., & May, J. 2006, ApJ, 641, 938
Maraston, C. 2005, MNRAS, 362, 799
Marigo, P., Girardi, L., Bressan, A., et al. 2008, A&A, 482, 883
Martinsson, T. P. K., Verheijen, M. A. W., Westfall, K. B., et al. 2013a, A&A, 557, A131
Martinsson, T. P. K., Verheijen, M. A. W., Westfall, K. B., et al. 2013b, A&A, 557, A130
Matthews, L. D., van Driel, W., & Gallagher, J. S., III 1998, AJ, 116, 2196
McClure-Griffiths, N. M., & Dickey, J. M. 2007, ApJ, 671, 427
McGaugh, S. S. 2005, ApJ, 632, 859
McGaugh, S. S. 2008, ApJ, 683, 137
McGaugh, S. S. 2011, PhRvL, 106, 121303
McGaugh, S. S. 2012, AJ, 143, 40
McGaugh, S. S., & de Blok, W. J. G. 1998, ApJ, 499, 41
McGaugh, S. S., & Schombert, J. M. 2014, AJ, 148, 77
McGaugh, S. S., Schombert, J. M., Bothun, G. D., & de Blok, W. J. G. 2000, ApJL, 533, L99
McGaugh, S. S., & Wolf, J. 2010, ApJ, 722, 248
McQuinn, K. B. W., Skillman, E. D., Berg, D., et al. 2013, AJ, 146, 145
Meidt, S. E., Schinnerer, E., van de Ven, G., et al. 2014, ApJ, 788, 144
Melbourne, J., Williams, B. F., Dalcanton, J. J., et al. 2012, ApJ, 748, 47
Milgrom, M. 1983, ApJ, 270, 371
Noordermeer, E., & Verheijen, M. A. W. 2007, MNRAS, 381, 1463
Oh, S., de Blok, W. J. G., Walter, F., Brinks, E., & Kennicutt, R. C. 2008, AJ, 136, 2761
Pfenniger, D., & Revaz, Y. 2005, A&A, 431, 511
Pizagno, J., Prada, F., Weinberg, D. H., et al. 2007, AJ, 134, 945
Portinari, L., Sommer-Larsen, J., & Tantalo, R. 2004, MNRAS, 347, 691
Rhode, K. L., Salzer, J. J., Haurberg, N. C., et al. 2013, AJ, 145, 149
Schechtman-Rook, A., & Bershady, M. A. 2014, ApJ, 795, 136
Schombert, J., Maciel, T., & McGaugh, S. 2011, AdAst, arXiv:1109.2360
Schombert, J., & McGaugh, S. 2014a, PASA, 31, 36
Schombert, J., & McGaugh, S. 2014b, PASA, 31, 11
Schombert, J., & Rakos, K. 2009, AJ, 137, 528
Sorce, J. G., Tully, R. B., & Courtois, H. M. 2012, ApJL, 758, L12
Stark, D. V., McGaugh, S. S., & Swaters, R. A. 2009, AJ, 138, 392
Swaters, R. A., Bershady, M. A., Martinsson, T. P. K., et al. 2014, ApJL, 797, L28
Swaters, R. A., Sancisi, R., van Albada, T. S., & van der Hulst, J. M. 2009, A&A, 493, 871
Trachternach, C., de Blok, W. J. G., McGaugh, S. S., van der Hulst, J. M., & Dettmar, R. 2009, A&A, 505, 577
Trujillo-Gomez, S., Klypin, A., Primack, J., & Romanowsky, A. J. 2011, ApJ, 742, 16
Tully, R. B., & Fisher, J. R. 1977, A&A, 54, 661
Tully, R. B., Pierce, M. J., Huang, J., et al. 1998, AJ, 115, 2264
Tully, R. B., Rizzi, L., Shaya, E. J., et al. 2009, AJ, 138, 323
Verheijen, M., & de Blok, E. 1999, Ap&SS, 269, 673
Verheijen, M. A. W. 2001, ApJ, 563, 694
Walter, F., Brinks, E., de Blok, W. J. G., et al. 2008, AJ, 136, 2563
Weiner, B. J., Willmer, C. N. A., Faber, S. M., et al. 2006, ApJ, 653, 1049
Zaritsky, D., Courtois, H., Muñoz-Mateos, J.-C., et al. 2014, AJ, 147, 134
Zibetti, S., Charlot, S., & Rix, H.-W. 2009, MNRAS, 400, 1181
Zibetti, S., Gallazzi, A., Charlot, S., Pierini, D., & Pasquali, A. 2013, MNRAS, 428, 1479